Estimates of North Atlantic Ventilation and Mode Water Formation for Winters 2002-2006

David S. Trossman
School of Oceanography, University of Washington, Seattle, WA

LuAnne Thompson
School of Oceanography, University of Washington, Seattle, WA

Kathryn A. Kelly
Applied Physics Laboratory, University of Washington, Seattle, WA

Young-Oh Kwon
Woods Hole Oceanographic Institution, Woods Hole, MA

In prep for *Journal of Physical Oceanography*, September 26, 2007

Short title: NORTH ATLANTIC VENTILATION

Abstract.

Lagrangian estimates for ventilation rates in the Gulf Stream Extension using Argo and World Ocean Circulation Experiment (WOCE)/Atlantic Climate and Circulation Experiment (ACCE) float data, scatterometer (QuikSCAT) wind stress satellite observations, and altimetric (Aviso) sea surface height (SSH) satellite observations from 2002 to 2006 are presented. Satellite winds and estimates of surface geostrophic currents allow the inclusion of the effects of currents on wind stress as well as their impact on the Ekman pumping. The presence of large surface geostrophic currents decrease the total Ekman pumping, contributing up to 20 % where the Gulf Stream makes its two sharpest turns, and increases the total Ekman pumping by 10 % or less everywhere else.

Using currents that are either climatological or vary from year to year and climatological MLDs (mixed-layer depths), obducted water tends to originate along the Gulf Stream, while subducted water tends to originate to its south. However, using time-varying MLDs for each year, water originating in the Sargasso Sea may either subduct or obduct. Vertical pumping is the only dominant factor in ventilation closer to the coast where MLDs are shallower and lighter parcels are subducted. Vertical pumping contributes up to 25% of the several hundreds of ventilated meters per year around the Gulf Stream and less elsewhere. The ageostrophic currents may be as large as 15% of the geostrophic currents, but only in region of the Gulf Stream. The horizontal and temporal structure of the MLDs is the primary factor that controls the hundreds of meters per year of ventilation (and a few Sverdrups of Eighteen Degree Water, EDW, subduction). EDW can reside in the thermocline for at least 3.5 years.

1. Introduction

In order to understand climate variability and water mass formation, it is important to know about water mass exchange rates between the surface and the thermocline. The ocean can exchange properties such as heat with the atmosphere and may store these properties for decades or longer through transfer to the thermocline (*Williams*, 2001). The upper ocean that separates the atmosphere and the permanent thermocline consists of an Ekman layer, a mixed layer, and a seasonal thermocline. Water parcels gain their identities in the mixed layer and keep their identities to a great extent in the thermocline.

It was believed by *Iselin* (1939) that Ekman pumping in the late winter (March) forced water to cross the base of the wind-generated Ekman layer and flow along isopycnals thereafter. *Stommel* (1979) hypothesized that taking all mixed layer parameters from late winter can bypass the complication of the seasonal cycle. Climatological estimates using Stommel's hypothesis assume water parcels subducted from the summer mixed layer are generally re-entrained as the mixed layer deepens the following winter. This is usually referred to as Stommel's mixed layer demon.

Ekman flow transports large amounts of heat in the ocean, and Ekman pumping, the divergence of this flow, drives large scale ocean circulation through the Sverdrup relation. However, estimates of Ekman pumping usually contain the assumption that surface geostrophic currents are negligible. In regions of strong currents, such as a western boundary current, this assumption is not valid. In these regions, not only do geostrophic currents influence the Ekman flow in the upper ocean, but they also modify Ekman pumping, which contributes to subduction (*Marshall et al.*, 1993).

Subduction is the mass flux from the seasonal thermocline into the permanent thermocline. Obduction is the (irreversible) mass flux into the seasonal thermocline from the permanent thermocline. These processes may also be referred to as ventilation. In addition to the sign difference, obduction and subduction are different in three ways, according to *Qiu and Huang* (1995): (1) Different physical processes govern them. Temperature and salinity

properties, as determined by the mixed layer processes, will be carried by the subducted water to the permanent thermocline. On the other hand, water loses its identity via convective mixing when water is obducted. (2) Subduction and obduction have different annual cycles. Subduction occurs after late winter when the mixed layer restratifies and obduction occurs between late fall and early winter when the mixed layer is deepening. (3) A mean annual subduction rate is an estimate of how much water enters the permanent thermocline, while a mean annual obduction rate is an estimate of how much water comes from the permanent thermocline.

Local maxima in the subduction of water occur where there are 'mode' waters. Mode water is nearly vertically homogeneous in density. The mode water of interest here is characterized by temperatures between 17 and 19^oC (*Worthington*, 1959). Because of this property, its alternate name is Eighteen Degree Water (EDW). This well-defined water mass is important for the storage and memory of heat in the North Atlantic. While surface heat fluxes largely determine the sea surface temperature (SST) variability in most of the World Ocean, heat transport makes as comparable contribution as surface heat fluxes in the northwestern North Atlantic (*Dong and Kelly*, 2004). This surface heat transport is typically thought to be driven by Ekman processes, but *Dong and Kelly* (2004) demonstrate how the largest interannual variations in oceanic heat storage are due to geostrophic heat transport via the Gulf Stream.

EDW is a link between the ocean and atmosphere. Production of EDW is believed to be connected to the North Atlantic Oscillation (NAO), sea surface density anomalies near the Gulf Stream, and deep water formation in the North Atlantic subpolar regions (*Curry and McCartney*, 2001). The EDW typically forms just south of the Gulf Stream, where it cools (to the lower end of the 17 to 19^oC range) and recirculates. Years with greater EDW production tend to have EDW closer to 17^oC while years with lower production have warmer EDW, as the EDW mixes with warmer recirculating water (*Kwon*, 2003). EDW is also an important component of the near surface overturning circulation and for transferring biogeochemical

properties between the near-surface and the ocean interior (since EDW is depleted of nutrients and rich in carbon content) (*Palter et al.*, 2005).

Joyce et al. (2000) found that the Gulf Stream (northern latitude) position, NAO index, and EDW potential vorticity (or lack of EDW production) are highly correlated with one another with a zero lag time. The EDW potential vorticity is also highly correlated with large-scale atmospheric forcing. Hence, three factors have been thought to influence EDW variability: (1) Gulf Stream position, (2) ocean-atmosphere heat fluxes, and (3) temperature and salinity anomaly advection. However, *Dong et al.* (2007) has found that both the oceanic advective convergence (which indicates the importance of (1) and (3)) and the product of heat fluxes and the area of the outcropping 17 to 19^oC isotherms (which indicates the importance of preconditioning), not variability of surface heat flux, play the most important roles in EDW variability. Since the NAO affects the SSTs, if the SSTs affect EDW volume then a link between the NAO and EDW may be drawn.

Kwon and Riser (2004) have shown that EDW volume reaches its annual peak in the winter. Using profile estimates, they show that the formation rate of EDW is on the order of $4 - 5$ Sv from profile estimates, as opposed to the $15 - 20$ Sv *Speer and Tziperman* (1992) estimated from air-sea fluxes. This discrepancy may be caused by an error in the Walin formulation (*Walin*, 1982) or inaccurate air-sea fluxes, but most probably can be accounted for by the eddy processes that result in lateral transport in the mixed layer near the Gulf Stream.

Here we build on the work of *Qiu and Huang* (1995) who made subduction rate estimates for the North Atlantic (and Pacific) with climatological estimates for MLDs, climatological estimates for currents, and *Hellerman and Rosenstein* (1983) wind stress data (which has been noted to overestimate the wind stress by 30% (*Harrison*, 1989)). We recalculate Ekman pumping, as *Xie* (2004) did with QuikSCAT wind stress data from 1999 to 2003, but including the impact of upper ocean geostrophic currents on Ekman velocities.

We include winds, currents, observationally-derived MLDs, and vertical shear to calculate ventilation rates and to estimate (EDW) ventilation. Section 2 describes the data we have used

in our Ekman pumping and ventilation rate estimates. Section 3 describes how we estimated (EDW) ventilation. We end with results before summarizing.

2. Data

Due to recent realizations of satellite and profiler systems, we are not only able to investigate inter-annual variability in a few selected locations, but intra-annual variability across the Gulf Stream and Sargasso Sea. QuikSCAT winds are available daily from July 1999 and mapped as in *Kelly et al.* (1999), Aviso SSHs are available weekly from October 1992, Argo temperatures and salinities are available every ten days from the year 2000, and WOCE/ACCE MLDs and temperatures are from 1997 through 2003. WOA (World Ocean Atlas of 1994) temperature and salinity climatologies are available for each month of the year. Our data is summarized in Table 1.

2.1. Surface Currents

The Aviso SSH product, on a $\frac{1}{3}^o \times \frac{1}{3}^o$ grid, also includes error maps which indicate significant errors located between the tracks of TOPEX/Poseidon and Jason-1. Because of these errors, surface geostrophic flow calculated from the SSH maps show signals that reflect the satellite track patterns. To address this track problem, we use spatial low-pass filtering on the SSH data after temporally averaging over three week blocks of time. In regions where the errors are greater than their corresponding SSH anomalies, we assumed that these SSH anomalies were zero, which were typically when errors exceeded 20 cm. The only places with greater errors are along the coast (sometimes as high as 50 cm). We use a half-power of six longitudinally (between 80 and 30^oW) and a half-power of five latitudinally (between 20 and 55^oN), low-pass filtering once in each direction with a Butterworth filter. We set our final SSH to be the sum of these low-passed anomalies and the mean Aviso SSH, derived from historical hydrographic and float (surface) data and provided by Aviso.

The resulting currents are derived from the geostrophic relationships

$$u_g = -\frac{g}{f}\frac{\partial \eta}{\partial y} \quad (1)$$

$$v_g = \frac{g}{f}\frac{\partial \eta}{\partial x}, \quad (2)$$

where $g = 9.81\frac{m}{s^2}$, f is the Coriolis parameter, and η is the SSH. These currents do not show a track pattern. Additional filtering was applied to mask over the jump between land and nonzero currents. If the difference between the currents between two grid points was $.25\frac{m}{s}$ and larger, then the currents from that longitude to the West-most grid point and within a box of three latitudinal grid points are set to zero. The mean annual geostrophic surface currents' structure maps out the Gulf Stream (left-hand side of Fig. 1). The objective map gives smaller SSH anomalies in regions of larger errors, which in turn gives smaller current speeds.

2.2. Shear

To obtain the vertical structure of the currents, we low-pass the potential densities averaged monthly from Jan. 2002 to Dec. 2006 using the same procedure as was used in low-pass filtering the SSH: once with a half-power of six longitudinally (between 80 and 30^oW) and a half-power of five latitudinally (between 20 and 55^oN). We find these potential densities using WOA (T,S) data when the errors associated with objectively mapped Argo (T,S) data exceed 0.5 of the true variance. Then we use the thermal wind equations,

$$\frac{\partial u_g}{\partial z} = \frac{g}{f\rho_o}\frac{\partial \rho_\theta}{\partial y} \quad (3)$$

$$\frac{\partial v_g}{\partial z} = -\frac{g}{f\rho_o}\frac{\partial \rho_\theta}{\partial x}, \quad (4)$$

where ρ_θ is the potential density and ρ_o is the mean density over our domain.

We grid these current shears with a fifty meter vertical resolution, vertically integrate, and use the Aviso surface currents from the previous section as a reference. The ratio of the currents at some depth to currents at the surface is capped at one, filled with the spatially averaged ratios for this depth if greater than one (which occurs at less than 10 % of grid

points). These currents are low-passed once in both horizontal directions with a half-power of four. Lastly, we fit analytical curves to the profiles of these ratios and low-pass with a half-power of four again for a small shear profile.

2.3. MLDs

The MLDs are calculated by using Argo and WOCE/ACCE data. The floats with World Meteorological Organization (WMO) identification number 852 from 2004 onward have been excluded due to a non-constant cold bias discovered in February of 2007 (http://argo.jcommops.org or for full documentation of the Argo system, http://www.coriolis.eu.org/cdc/argo_rfc.htm). These floats were fairly uniformly distributed in the North Atlantic. Thus, while we expect the MLDs to be biased low including these data and to be higher excluding these data, the MLDs should be better with their exclusion. The criterion we use to determine the MLDs is $\Delta T > 0.3^oC$. Here, ΔT is the difference between the surface in situ temperature and the in situ temperature at some depth. We are not using density as a criterion because salinity is not routinely measured, other than by the Argo system. The minimum depth at which our criterion holds is what we call the MLD.

The MLDs were objectively mapped from the pressures. We use the method of *Le Traon* (1990), building on the work of *Bretherton et al.* (1976). We set our large scale basis function to be $1 + x + y + x^2 + y^2$, use a Poissonian covariance function, and use a decorrelation length scale of 150 kilometers. An average of our MLDs from 2002 to 2006 for each month was used to more accurately derive the MLDs in region of large error (as big as 200% of the true variance along the borders and coast). The MLD, h_t, at a given point has been replaced with $h_t - \frac{|h_t - h_{clim}||\varepsilon_t - \varepsilon_{max}|}{\varepsilon_{max}}$ if the error is exceeds $\varepsilon_{max} = 100\%$. Here, h_{clim} are the Argo-derived, average, monthly MLDs from 2002 to 2006 and ε_t are the associated errors in units of percent of the true variance.

The boundary between the seasonal and permanent thermoclines is defined to be the maximum MLD over one year time. Here, one year is the time from when the MLD is deepest

one year to when the MLD is deepest in the next year, at each horizontal grid point. This can be shorter or longer than one year and this variability of time between maximum MLDs greatly influences the result.

3. Methods

3.1. Ekman Pumping

The ageostrophic currents are small in most places relative to the geostrophic ones (right-hand side of Fig. 1). The first-order correction ageostrophic currents only get up to 15.8% of the geostrophic currents at any given place or time and almost never get above 10%. The greatest geostrophic current contributions to the Ekman transports come from terms with derivatives in the geostrophic flow (e.g. $U_e \frac{\partial u_g}{\partial x}$). The contribution from the derivatives in the Ekman transports are negligible, especially outside of the Gulf Stream.

Ekman pumping is defined by $-w_e \equiv -\vec{\nabla} \cdot \vec{U_e}$, as a convergence of Ekman transports, $\vec{U_e}$, which leads to a downward motion. Usually, the Ekman transports are approximated with wind momentum input uncoupled from currents:

$$U_e = \frac{1}{\rho}\frac{\tau^y}{f} \tag{5}$$

$$V_e = -\frac{1}{\rho}\frac{\tau^x}{f}, \tag{6}$$

here, called the simple Ekman balance (Appendix). This analytical approximation, which *Qiu and Huang* (1995) and *Xie* (2004) have used for w_e, is valid in most regions, but the assumptions fail in the Gulf Stream. If surface geostrophic currents are strong then the vertically averaged flow in the Ekman layer satisfies:

$$U_e\frac{\partial u_g}{\partial x} + u_g\frac{\partial U_e}{\partial x} + V_e\frac{\partial u_g}{\partial y} + v_g\frac{\partial V_e}{\partial y} - fV_e = \frac{\tau^x}{\rho} - \tau_{damp}U_e \tag{7}$$

$$U_e\frac{\partial v_g}{\partial x} + u_g\frac{\partial V_e}{\partial x} + V_e\frac{\partial v_g}{\partial y} + v_g\frac{\partial U_e}{\partial y} + fU_e = \frac{\tau^y}{\rho} - \tau_{damp}V_e. \tag{8}$$

We have used the approximation of *Qiu and Huang* (1995) and *Xie* (2004) for a first guess to the Ekman pumping. We also impose the simple Ekman balance at the coasts. Such regions

serve as boundaries to the regions in which the *Qiu and Huang* (1995) approximation is not valid and help define a well-posed problem. To numerically solve for a converged solution, we have applied a time difference method with time steps, $\Delta t = 1/2hr$. We applied these steps in time in an iterative fashion, including accelerations as well as damping terms, $\tau_{damp}U_e$ and $\tau_{damp}V_e$, with $\tau_{damp} = 1$ day^{-1} (still several times shorter than our temporal resolution). A convergent steady solution was found. The geostrophic currents are held fixed for each week of Aviso SSH data and QuickScat wind data. This yields the Ekman currents, and from this, we calculate w_e.

3.2. Parcel Tracking

Following the method of *Qiu and Huang* (1995), fluid parcels are tracked from a given initial position and time until they are obducted or run into the coast, with time steps of seven days. We track the parcel within the upper 1000 meters, and within the domain of $27 - 53^o$N and $78 - 32^o$W. The parcels are placed on a 2^o latitude by 2^o longitude by $100 - 200$ meters depth grid system and tracked for each vertical grid point, due to run-time constraints. If the deepest MLD is greater than 600 meters, a 200 meter depth resolution is used; if the deepest MLD is greater than 400 meters, a 150 meter resolution is used; and otherwise, a 100 meter resolution is used. The only purpose of this grid is to resolve the vertical shear in the geostrophic flow.

To track the parcels, a fourth-order Runge-Kutta integration was used. The numerical time intergrations were performed with Matlab's `ode45` (fourth-order Runge-Kutta) routine at a relative tolerance of 1%. This integration was on the velocities along the trajectory of each water parcel, $u_{tr} = \frac{u_g}{111200}$, $v_{tr} = \frac{v_g}{111200 sin(\frac{\pi\lambda}{180})}$, and

$$w_{tr} = \begin{cases} w_e z/\delta_e + \frac{\beta}{f}\int_{-z}^{0} v_g dz' & \text{if } 0 > z > \delta_e \\ w_e + \frac{\beta}{f}\int_{-z}^{0} v_g dz' & \text{if } \delta_e > z \end{cases}$$

where λ is degrees latitude, $\delta_e = 40$ meters is the Ekman layer depth, 111200 is the conversion factor from $\frac{m}{s}$ to $\frac{degrees}{s}$, f is the Coriolis parameter, and β is the latitudinal derivative of f.

Finally, we assume that flows just below the mixed layer are geostrophic.

We find the depths at which parcels first cross h_m, the permanent thermocline depth, to find the thickness of the water column that gets transferred over the period of time it takes for the mixed layer to be deepest from one year to the next. We stop tracking parcels that go outside of our model domain and assume that the water parcels do not subduct if they are above the MLD when this occurs. Obduction can be similarly defined where the water parcels are entrained, instead of detrained (Fig. 2). Ultimately, we find the deepest and shallowest depths at which water parcels subduct and obduct on a 50 m vertical grid. We performed the same calculation with a 10 meter resolution and obtained results that were different by at most $10\frac{m}{yr}$, less than our error.

We use a true variance of 10000 m^2 for the MLDs, estimated from the variance in our data, to find the errors for two consecutive years, $h_{m,0,err}$ and $h_{m,1,err}$ (Fig. 3, center). To get an error estimate in ventilation, we propagate these errors with $\Delta h_{err} = (h^2_{m,0,err} + h^2_{m,1,err})^{\frac{1}{2}}$ and divide by the time from when the MLDs are a maximum one year to the next, T. This yields $\frac{1}{T}\Delta h_{err}$ which we compare with $\frac{1}{T}\Delta h_m$, the lateral induction term in the *Qiu and Huang* (1995) formulation (16).

3.3. Parcel Identities

Mixing is taken into account by letting water parcel properties (temperature, salinity, etc.) be set at the base of the mixed-layer and below. A parcel's properties, once in the permanent thermocline, are very close to those when and where they subduct in our Lagrangian trajectory calculation so a parcel's properties are set once out of the mixed layer. If a parcel comes back into the mixed-layer, we cannot assume that it conserves its properties.

We calculate the vertical thickness of water between 17 and 19^oC in the permanent thermocline and multiply by the area of a grid cell at each grid point to find the volume of EDW in a given month from objectively mapped thicknesses of Argo profiler temperature data. This objective mapping procedure is the same as the one for the MLDs. We do not use

WOA data substitutions because this reduces the seasonal variability in the record. *Kwon and Riser* (2004) imposes an eastern boundary of 40^oW and a southern boundary of 25^oN, a matter of convention, onto his region to calculate EDW volume, which we use here as well.

By tracking how much water is between 17 and 19^oC as it enters the permanent thermocline each year, we can calculate the mean annual EDW subduction rates. We do the same with EDW exiting the permanent thermocline to get the mean annual EDW obduction rates. We use the objectively mapped temperatures from Argo and WOCE/ACCE data to define the EDW.

4. Results

4.1. Ventilation analysis

By taking advantage of new data sets, we are able to make new estimates for the quantities needed to estimate the ventilation of the thermocline in the North Atlantic. Accounting fully for the geostrophic currents numerically, w_e is noticeably different from that using in the usual approximation scheme in which winds only, and not geostrophic currents, are taken into account (Fig. 4). The advection of Ekman velocities by geostrophic currents make about a 20% decrease in the w_e where the Gulf Stream makes its sharpest turns (consistent with our ageostrophic velocities being largest there). The Ekman velocities increase w_e by about a 10% elsewhere. Comparing our w_e with *Xie* (2004), who also used QuikSCAT winds, we see similar structure and magnitude, whereas w_e of *Qiu and Huang* (1995) is only half as big in the Gulf Stream. In particular there is less pumping south of the Gulf Stream, in the Sargasso Sea, and less suction north of the Sargasso Sea.

Parcels travel at most five degrees latitudinally but may travel as many as twenty degree longitudinally in a year. Lateral induction, $\frac{1}{T}\Delta h_m$, (Appendix) dominates both subduction and obduction away from the coast, contributing a few hundreds of meters per year while vertical transport contributes at most $75\ \frac{m}{year}$ in the *Qiu and Huang* (1995) formulation (16). However,

vertical transport becomes quite significant closer to the coasts.

With shear in weekly currents and monthly MLDs for individual years from 2002 to 2005, our maximum and root mean squared ventilation rates were compared with the *Qiu and Huang* (1995) formulation and their associated errors (Table 2 and Fig. 5). Using the simplified formulation, the errors are much less than ventilation estimates. The error estimates serve as an upper bound on the errors in our Lagrangian trajectory model in part because the ventilation calculated using (16) is greater than found in our model. Also, the regions with the largest errors are on the fringes of our domain, near the coasts and on the borders of our maps.

A concern is whether the trends in Table 2 are an artifact of better data coverage in later years. The number of non-zero points the MLDs are objectively mapped onto are maximum in 2004 because the WMO identification number 852 floats increased from 2004 to 2006 and have been taken out of this analysis. The number of points the objective mapping routine uses to describe the data are 1475 in 2002, 1571 in 2003, 1582 in 2004, 1503 in 2005, and 1437 in 2006. Furthermore, the regions with the largest errors are the later years, but most of the subduction occurs in regions with relatively low errors (Fig. 3, center).

Vertical shear in the geostrophic flow has a second-order effect on the ventilation rates. This shear may cause up to a 10% decrease in ventilation, but is not clearly out of our range of error. To see this, an average monthly MLD climatology was constructed over 2002 to 2006 and used to calculate ventilation both with and without shear (Fig. 6). By taking the monthly average of the Argo-derived MLDs over 2002-2006, mean annual currents with shear, and mean annual vertical velocities, we can compute climatological ventilation rates. Then we can compare this to the ventilation rates we get by using the monthly Argo-derived MLDs (not averaged over 2002-2006), mean annual currents with shear, and mean annual vertical velocities, and finally taking the average of these ventilation rates over 2002-2006. We find that the ventilation rates calculated using mean currents and/or mean MLDs are significantly smaller (Fig. 7). This non-linearity in the problem mostly comes from the constituents of the lateral induction term.

The MLDs are not deepest in March every year (Fig. 3, bottom). For example, one year may have a deepest MLD in April and the next may have a deepest MLD in February at a given horizontal grid point, as governed by convective cooling and stratification strength. Then Δh_m may not compensate for this decrease in T by decreasing in concert. The MLDs within the Gulf Stream are not as deep as they are to its south and east; while the stratification is mostly weak within the Gulf Stream, the negative buoyancy forcings are sufficiently counteracted by advected heat.

The subduction rates are nonzero south and east of the Gulf Stream where the MLDs deepen most (Fig. 3, top). Their magnitudes are consistent with *Qiu and Huang* (1995). On the other hand, some deep MLDs appear from nothingness in the southern part of our domain in some years (particularly in years with the largest errors: 2002 and 2006). This suggests a lack of adequate sampling coverage in this region. With sufficient MLD variability, water could be subducted and then obducted in a period of time shorter than a year. We cannot estimate how long water parcels reside in the thermocline after subduction because we only have four years of data that may be tracked. However, we see that some of the parcels that reside in the thermocline for more than a year can be identified as EDW.

4.2. Density class analysis

The volume transport rates in our domain for σ_θ up to 28.2 $\frac{kg}{m^3}$ are in Table 3. The subducted waters come from regions South and Southeast of the Gulf Stream, while obducted waters come from regions along the Gulf Stream and closer to shore. Most of the subducted waters are slightly less dense than the obducted waters (Fig. 8), consistent with *Qiu and Huang* (1995). There is a skewed Gaussian-shaped distribution of ventilation as a function of density and two peaks in subduction for most years. The reason for this double peak in subduction is the local subduction minimum in the 27.2 σ_θ density class (seen in 2002 and 2004), consistent with observations that there is a local minimum in oxygen concentration there (*Richards and Redfield*, 1955).

Waters denser than EDW, of 27.0 $\frac{kg}{m^3}$ and above, are subducted where the ageostrophic currents are relatively large on an annual average as well as on a winter average, accelerating the subduction process into the Gulf Stream. Waters less dense than 22.2 $\frac{kg}{m^3}$ subduct in areas where MLDs are relatively shallow and Ekman pumping is relatively strong; in particular, along the coast (Fig. 9). While subduction of the lightest waters in the slope region is consistent with the model of *Speer and Tziperman* (1992), this is the region where the errors in the Argo data are largest. The presence of water below 22.2 $\frac{kg}{m^3}$ may be an exaggeration of how light this water is. Lastly and also consistent with the model of *Speer and Tziperman* (1992), we found that Ekman pumping makes a negligible contribution to ventilation where EDW subducts (Fig. 10).

4.3. EDW formation charactistics

The density range between 26.2 and $27.6\frac{kg}{m^3}$ accounts for most of the ventilated waters as well as the newly subducted EDW in the Sargasso Sea except in 2003. Most of the ventilated EDW lies within the range of σ_θ between 26.0 and $26.8\frac{kg}{m^3}$. This is consistent with the EDW densities of *McCartney and Talley* (1982). In 2003, the density range of ventilated EDW shifted to lower density classes and spread out. This may be explained by EDW that was formed in previous years being subducted in 2003.

EDW is found to form just south of the Gulf Stream. This subtropical mode water follows the North Atlantic recirculation gyre towards the south and subducts towards the edges of the recirculation gyre with a higher population of water between 17 and 19^oC during springtime (Fig. 10). We find that there is weaker stratification at the top of the thermocline where there is EDW. There is virtually no EDW north of the Sargasso Sea because older EDW mixes and is modified by heat fluxes after entering the Gulf Stream. The rest of the water between 17 and 19^oC is of subpolar origin.

We find EDW subduction rates closer to that of *Kwon and Riser* (2004) than *Speer and Tziperman* (1992). Indeed, it appears as though the *Walin* (1982) formulation accounts only

for wintertime formation. More water between 17 and 19^oC is formed than subducts (Table 3). The difference between the EDW formation rates of *Kwon and Riser* (2004) and *Speer and Tziperman* (1992) appear to the explained by the difference between the mean annual volume of water between 17 and 19^oC and EDW volume. Our EDW subduction and obduction rates are also tabulated in Table 3. It is apparent that a net positive subduction rate of EDW does not necessarily indicate an increase in EDW volume and similarly a net positive obduction rate of EDW does not dictate a decrease in EDW volume. The missing EDW from this picture is both EDW that is modified in the Gulf Stream and EDW that is not modified after obducting.

The spatial distribution of the errors in EDW volume is the same as that of the MLDs (Fig. 3, center) because the same objective mapping procedure was applied to the EDW thicknesses themselves. By estimating the thickness of water between 17 and 19^oC via objectively mapped Argo temperatures, we find similar volumes to the thickness objective mapping procedure until 2005 and 2006 when the thickness objective mapping procedure yields EDW volumes that are twice as large. The spatial distributions of EDW and seasonal variability between 3×10^{14} m^3 to almost 8×10^{14} m^3 are robust. Using a combination of objectively mapped temperatures from both Argo and WOA data yields EDW volumes with a depressed seasonal variation.

Over our four years, there is an mean obduction of 14 Sv of water, with 2002 and 2003 having more obduction and 2004 and 2005 have more subduction. Subducted waters are about the same density on average as obducted waters. However, obducted waters are generally warmer relative to their surroundings than subducted waters. Similarly, since EDW is cold relative to surrounding waters in the mixed layer, we find a warm anomaly due to EDW in the mixed layer in the Sargasso Sea for 2002 and 2003 and a cold anomaly in the mixed layer in the Sargasso Sea due to EDW in 2004 and 2005.

4.4. EDW, NAO, and MLDs discussion

Because of the short record in our analysis, our study does not contribute to understanding the processes that control the 10-20 year time scale that has been proposed to be important for NAO variability. The estimates for a decadal peak in the NAO include both observational studies (a nine year, pre-1945, period *Grötzner et al.* (1998), a twelve year, post-1945 and pre-late 1990's, period *Grötzner et al.* (1998)), and modeling studies (seventeen years from *Grötzner et al.* (1998), twelve to sixteen year period from *Wu and Liu* (2005), or twelve year period from *Marshall et al.* (2001)).

We might expect that integrated NAO might correlate with EDW volume as the ocean responds to integrated atmospheric forcing over a time scale controlled by the renewal time of the EDW. *Curry and McCartney* (2001) estimated a three to five year renewal time of EDW while *Joyce et al.* (2000) estimated a five to seven year lag time for the Labrador Sea Water signal to be seen in the Sargasso Sea. *Kwon* (2003) found a lag time between one and six years between integrated NAO index with EDW volume and MLDs just south of the Gulf Stream. *Joyce et al.* (2000) also suggested that there is a link between the Gulf Stream's position and the (integrated) NAO.

To understand how the NAO can influence EDW and heat storage in the ocean, consider a period of time with the integrated NAO is less positive, there are weaker westerlies as well as a more zonal and southern storm track. The result is less wintertime buoyancy loss over the EDW formation region. Wintertime winds tend to positively correlate with the wintertime (non-integrated) NAO index over the EDW formation region. With weaker winds, less buoyancy loss creates a shallower boundary between the permanent and seasonal thermocline, h_m, south of where the Gulf Stream branches. There will be less EDW formation at this time (above h_m) due to less deep convection. Newly produced EDW is cold relative to older EDW in the subropical recirculation gyre so there will be a warm temperature (or negative density) anomaly with a dearth of EDW.

In the following years, if more EDW is advected into the southern Sargasso Sea, h_m

may shallow. The MLDs (and h_m for the year) are relatively deep just south of the Gulf Stream and relatively shallow in the southern Sargasso Sea in the years, such as 2004 and 2005, following a cumulative weak NAO forcing. There will be relatively new (cold) EDW subducting in years such as 2004 and 2005 because h_m will have become shallower for a number of years in the southern Sargasso Sea and subducted EDW formed in previous years. Once the cold EDW subducts, its temperature is conserved, carrying its low potential vorticity downstream. A less stratified water column directly below h_m where EDW accumulates will remain. Ultimately, the subsurface temperatures modify the SSTs and EDW gets mixed in the Gulf Stream, modifying the heat fluxes and transport. It is possible that these processes alter the NAO index as a negative feedback, producing the oscillation, but this goes into the realm of speculation. An accumulative large NAO index may be argued to produce the opposite of the aforementioned scenario.

This is not inconsistent with the mechanism *Joyce et al.* (2000) proposed. The deepening of the MLDs to the right of the geostrophic currents (e.g. the Gulf Stream) couples the Gulf Stream position with the MLDs. Also in support of the above is the anti-correlation between the (integrated) NAO index and mixed layer temperatures found by *Kwon* (2003). However, there are confounding factors such as the Gulf Stream's position, how the SSTs may be otherwise affected, the El Nino Southern Oscillation, the Arctic Oscillation, and the Pacific Decadal Oscillation. These, we hypothesize, explain most of the less-than-perfect correlation at the oscillation period. Further studies need to be accomplished on this as well as the influence of EDW on heat fluxes and transport.

5. Conclusions

The geostrophic currents contribute significantly to the associated relative velocities of the winds to yield the wind stresses. This affects the Ekman divergences by about $10 - 20\%$ as well as the Sverdrup transports. However, vertical pumping is increasingly negligible relative to lateral induction farther away from the coast. Including a small vertical shear can

make about a 10% difference in ventilation rates, albeit on the order of our error. There is a non-linearity in the Lagrangian estimates of ventilation rates. This renders 'analytical' calculations to be overestimates and the use of climatologies in methods similar to our Lagrangian trajectory method to be underestimates.

Subducted waters tend to come from south of the Gulf Stream, while obducted waters come from along the Gulf Stream. The lightest waters subduct at the coast where vertical velocities can dominate MLD variability. Water heavier than EDW is aided by the ageostrophic currents in subduction more than other waters. Both lateral induction and vertical pumping are non-negligible in the Gulf Stream. MLD variability matters most for ventilation elsewhere. A more weakly stratified thermocline boundary in the Sargasso Sea may be due to EDW ventilation.

WOA data have been used in related studies (e.g. *Kwon* (2003) and *Joyce et al.* (2000)), but due to the relatively unpronounced seasonal variability in WOA data, the temporal resolution made possible by the Argo system allows us to investigate variability at higher frequencies. The importance of intra-annual variations in MLDs, for instance, must be emphasized in estimating EDW ventilation rates. These rates are greatest during the springtime when the mixed layer shallows. Some of the subducted EDW resides in the thermocline for a period longer than the length of our time series: at least 3.5 years. This warrants future investigations because the EDW residence time may play a crucial role in a potential NAO-EDW coupled oscillation.

SST anomalies, as forced by mixed layer temperature anomalies and the NAO via heat transport and surface heat fluxes, may connect some of the dots between EDW and the NAO. It has long been thought that the current anomalies carrying background temperatures ($u'\overline{T}$) are primarily responsible for heat transport in the North Atlantic subtropical gyre, but temperature anomalies carried by background currents ($\overline{u}T'$) may be important in regions populated by EDW (i.e. the Sargasso Sea). However, further analysis is needed to tie together the feedback loop; that is, how EDW may modify the Gulf Stream and in turn modify the sea level pressure

in particular.

6. Appendix

Starting from the momentum-balance equations for an incompressible fluid and neglecting viscosity, we have the set of coupled partial differential equations (PDEs),

$$\frac{\partial u}{\partial t} + u\frac{\partial u}{\partial x} + v\frac{\partial u}{\partial y} + w\frac{\partial u}{\partial z} - fv = \frac{1}{\rho}\frac{\partial \tau^x}{\partial z} - \frac{1}{\rho}\frac{\partial p}{\partial x} \tag{9}$$

$$\frac{\partial v}{\partial t} + u\frac{\partial v}{\partial x} + v\frac{\partial v}{\partial y} + w\frac{\partial v}{\partial z} + fu = \frac{1}{\rho}\frac{\partial \tau^y}{\partial z} - \frac{1}{\rho}\frac{\partial p}{\partial y} \tag{10}$$

where the zonal, meridional, and vertical currents are $u = u_e + u_g$, $v = v_e + v_g$, and $w = w_e$, respectively, the sums of their Ekman and geostrophic contributions. Thus, by vertically integrating over the Ekman layer with depth, δ_e, we get the set of coupled PDEs,

$$\begin{aligned} \frac{\partial(U_e + \delta_e u_g)}{\partial t} + \int_{-\delta_e}^{0} u_e\frac{\partial u_e}{\partial x}dz + U_e\frac{\partial u_g}{\partial x} + u_g\frac{\partial U_e}{\partial x} + \delta_e u_g\frac{\partial u_g}{\partial x} + \\ \int_{-\delta_e}^{0} v_e\frac{\partial u_e}{\partial y}dz + V_e\frac{\partial u_g}{\partial y} + v_g\frac{\partial U_e}{\partial y} + \delta_e v_g\frac{\partial u_g}{\partial y} + \int_{-\delta_e}^{0} w_e\frac{\partial u}{\partial z}dz - fV_e + fV_a &= \frac{\tau^x}{\rho} \end{aligned} \tag{11}$$

$$\begin{aligned} \frac{\partial(V_e + \delta_e v_g)}{\partial t} + \int_{-\delta_e}^{0} u_e\frac{\partial v_e}{\partial x}dz + U_e\frac{\partial v_g}{\partial x} + u_g\frac{\partial V_e}{\partial x} + \delta_e u_g\frac{\partial v_g}{\partial x} + \\ \int_{-\delta_e}^{0} v_e\frac{\partial v_e}{\partial y}dz + V_e\frac{\partial v_g}{\partial y} + v_g\frac{\partial V_e}{\partial y} + \delta_e v_g\frac{\partial v_g}{\partial y} + \int_{-\delta_e}^{0} w_e\frac{\partial v}{\partial z}dz + fU_e + fU_a &= \frac{\tau^y}{\rho} \end{aligned} \tag{12}$$

where here 'a' denotes ageostrophic, the integrated zonal Ekman currents are U_e and the intergrated meridional Ekman currents are V_e, and the ageostrophic non-Ekman transports are U_a and V_a. These reduce to Equations 7 and 8 after introducing τ_{damp} to iteratively find a solution.

Now we apply the following assumptions: (a) The geostrophic currents are vertically uniform in the Ekman layer, which is reasonable if we assume the Ekman layer depth is finer than our vertical resolution. (b) The geostrophic currents obey quasi-geostrophic dynamics. That is, $\frac{\partial u_g}{\partial t} + u_g\frac{\partial u_g}{\partial x} + v_g\frac{\partial u_g}{\partial y} - fv_a = 0$ and $\frac{\partial v_g}{\partial t} + u_g\frac{\partial v_g}{\partial x} + v_g\frac{\partial v_g}{\partial y} + fu_a = 0$ to first-order. This essentially assumes that Rossby number, $Ro = \frac{U}{fL}$, is much less than unity. The ageostrophic current terms are of order Ro compared to the geostrophic velocities. Also, the vertical

velocity, w, is of the order of Ro compared to aspect ratio scaling. (c) Terms to second order in u_e and v_e (e.g. $\int_{-\delta_e}^{0} dz u_e \frac{\partial u_e}{\partial x}$) are negligible. The Ekman currents are so smooth that, in fact, all first-order derivatives of them are negligible.

We can solve for the Ekman transports, U_e and V_e, explicitly if we make further assumptions about the strengths of the Ekman and geostrophic currents and their derivatives in space with respect to one another: If (d) $\frac{(\frac{\partial u_e}{\partial x})}{(\frac{\partial u_g}{\partial x})} \ll 1$ and (e) $\frac{u_g}{u_e} \ll 1$ (similarly for derivatives in y and for the meridional currents) then we get,

$$U_e \approx \frac{1}{\rho}\left(\frac{\tau^x \frac{\partial v_g}{\partial y}}{(f(f + \frac{\partial v_g}{\partial x} - \frac{\partial u_g}{\partial y}))} + \frac{\tau^y}{(f + \frac{\partial v_g}{\partial x})}\right) \tag{13}$$

$$V_e \approx \frac{1}{\rho}\left(\frac{\tau^y \frac{\partial u_g}{\partial x}}{(f(f + \frac{\partial v_g}{\partial x} - \frac{\partial u_g}{\partial y}))} - \frac{\tau^x}{(f - \frac{\partial u_g}{\partial y})}\right). \tag{14}$$

From these analytical results, we can find $w_e = \frac{\partial U_e}{\partial x} + \frac{\partial V_e}{\partial y}$ to get,

$$w_e \approx \frac{1}{\rho}\frac{1}{(f + \frac{\partial v_g}{\partial x} - \frac{\partial u_g}{\partial y})}\left(\frac{\partial \tau^y}{\partial x} - \frac{\partial \tau^x}{\partial y} - \frac{\beta}{f}\tau^x - \frac{\beta}{(f + \frac{\partial v_g}{\partial x} - \frac{\partial u_g}{\partial y})}\right.$$
$$\left.\times((\tau^y - \tau^x)(\frac{\partial v_g}{\partial x} - \frac{\partial u_g}{\partial y}) + 2(f(\tau^y - \tau^x) - \tau^x(\frac{\partial v_g}{\partial x} - \frac{\partial v_g}{\partial y}) + \tau^y(\frac{\partial u_g}{\partial x} - \frac{\partial u_g}{\partial y})))\right). \tag{15}$$

It is assumption (e) that fails almost everywhere, but this is our first guess in numerically solving for the Ekman currents. Note that a negative value for w_e represents water transport from the Ekman layer down to the mixed layer because of how we have defined this quantity. A positive Ekman suction is a positive w_e and a positive Ekman pumping is a negative w_e.

Subduction rates are oriented oppositely to w_e, which can be seen in the expression the mean annual subduction rates have typically been approximated:

$$S_{ann} = -\overline{(w_e - \frac{\beta}{f}\int_{-\delta_e}^{0} v_g dz)} + \frac{1}{T}(h_{m,0} - h_{m,1}). \tag{16}$$

Here, T is one year and $h_{m,0}$ and $h_{m,1}$ are the March MLDs for the year in which we want to compute the mean subduction rate and the year after that, respectively. The first term represents vertical pumping and the second term represents lateral induction. Average rates of obduction may be computed similarly but with MLD information about one year and the one

previous to it, instead of following it. Eulerian ventilation rate calculations yield information about where (opposed to from where) and how much water is ventilated. Over a period, T, an average subduction rate has usually been computed via:

$$S_{avg} = -\frac{1}{T}\int_{t_0}^{t_1} w_{tr} dt - \frac{1}{T}\int_{t_0}^{t_1} (\frac{\partial h}{\partial t} + u_{tr}\frac{\partial h_m}{\partial x} + v_{tr}\frac{\partial h_m}{\partial y}) dt \tag{17}$$

where t_0 is the initial time, t_1 is the final time (hence $T = t_1 - t_0$), w_{tr} and (u_{tr}, v_{tr}) are the vertical and horizontal velocities along the trajectory, h_m is depth of the mixed layer, and the $\frac{\partial h}{\partial t}$ term is assumed to average out to zero.

Acknowledgments.

The authors would like to acknowledge Suzanne Dickinson for preparing the QuikSCAT gridded wind speed field, and Li Ren for some of the Argo data.

QuikSCAT winds are available at:
http://podaac-www.jpl.nasa.gov/cgi-bin/dcatalog/fam_summary.pl?ovw+qscat.

Aviso SSHs are available at:
http://www.aviso.oceanobs.com/html/donnees/produits/hauteurs/global/msla_uk.html.

Argo temperatures and salinities are available at:
http://www.usgodae.org/ftp/outgoing/argo/geo/atlantic_ocean.

WOA temperature and salinity climatologies are available at:
http://www.cdc.noaa.gov/cdc/data.nodc.woa94.html.

References

Bretherton, F. P., R. E. Davis, and C. B. Fandry, 1976, A technique for objective analysis and design of oceanographic experiments applied to MODE-73. *Deep-Sea Res.*, **23**, 559–582.

Curry, R. G., M. S. McCartney, and T. M. Joyce, 1998, Oceanic transport of subpolar climate signals to mid-depth subtropical waters. *Nature*, **391**, 575–577.

Curry, R. G. and M. S. McCartney, 2001, Ocean Gyre Circulation Changes Associated with the North Atlantic Oscillation, *J. Phys. Ocean.*, **31**, 3374–3400.

Dong, S., K. Kelly, Heat Budget in the Gulf Stream Region, 2004: The Importance of Heat Storage and Advection, *J. Phys. Ocean.*, **34**(05), 1214–1231.

Dong, S., S. L. Hautala, K. A. Kelly, 2007: Interannual Variations in Upper Ocean Heat Content and Heat Transport Convergence in the Western North Atlantic, *J. Phys. Oceanogr.*, in press.

Harrison, D. E., 1989; On climatological monthly mean wind stress and wind stress curl fields over the World Ocean. *J. Climate*, **2**, 57–70.

Grötzner, A., M. Latif, T. P. Barnett, 1998; A Decadal Climate Cycle in the North Atlantic Ocean as Simulated by the ECHO Coupled GCM. *J. Climate*, **11**, 831–847.

Hellerman, S., M. Rosenstein, 1983: Normal monthly wind stress over the world ocean with error estimates, *J. Phys. Ocean.*, **13**, 1093–1104.

Huang, R. X., B. Qiu, 1994: Three-Dimensional Structure of the Wind-Driven Circulation in the Subtropical North Pacific, *J. Phys. Ocean.*, **24**(07), 1608–1622.

Kelly, K. A., S. Dickinson, and Z.-J. Yu, 1999: NSCAT tropical wind stress maps: Implications for improving ocean modeling, *J. Geophys. Res.*, **104**(11), 11,291–11,310.

Kelly, K. A., S. Dickinson, M. J. McPhaden, and G. C. Johnson, 2001: Ocean currents evident in satellite wind data, *Geophys. Res. Lett.*, **28**(12), 2469–2472.

Kwon, Y.-O., 2003: Observation of General Circulation and Water Mass Variability in the North Atlantic Subtropical Mode Water Region. PhD Dissertation, *University of Washington*, Seattle.

Kwon, Y.-O., S. Riser, 2004: North Atlantic Subtropical Mode Water: A history of ocean-atmosphere interaction 1961-2000, *Geophys. Res. Lett.*, **31**(10), L19307.

Iselin, C. O. .D., 1939: The influence of vertical and lateral turbulence on the characteristics of the waters at mid-depths, *Trans. Amer. Geophys. Union*, **28**(20), 1–26.

Joyce, T. M., C. Deser, M. A. Spall, 2000: The Relation between Decadal Variability of Subtropical Mode Water and the North Atlantic Oscillation, *J. Climate*, **13**, 2550-2569.

Le Traon, P. Y., 1990, A Method for Optimal Analysis of Fields With Spatially Variable Mean. *J. Geophys. Res.*, **93**(8), 13,543–13,547.

Marshall, J. C., A. J. George Nurser, R. G. Williams, 1991: On the Relationship between Subduction Rates and Diabatic Forcing of the Mixed Layer, *J. Phys. Ocean.*, **21**(12), 1793–1802.

Marshall, J. C., A. J. George Nurser, R. G. Williams, 1993: On the Relationship between Subduction Rates and Diabatic Forcing of the Mixed Layer, *J. Phys. Ocean.*, **23**(07), 1315–1329.

Marshall, J., H. Johnson, and J. Goodman, 2001: A Study of the Interaction of the North Atlantic Oscillation with Ocean Circulation. *J. Climate*, **14**, 1399–1421.

McCartney, M. S. and L. D. Talley, 1982: The subpolar mode water of the North Atlantic Ocean, *J. Phys. Oceanogr.*, **12**, 1169–1188.

Palter, J. B., M. S. Lozie, R. T. Barber, 2005: The effect of advection on the nutrient reservoir in the North Atlantic subtropical gyre. *Nature*, **437**, 687–692.

Qiu, B., R. X. Huang, 1995: Ventilation of the North Atlantic and North Pacific: Subduction Versus Obduction, *J. Phys. Ocean.*, **25**(10), 2374–2390.

Richards, F. A., A. C. Redfield, 1955: Oxygen-density relationships in the western North Atlantic Ocean. *Deep-Sea Res.*, **2**, 182–189.

Seager, R., Y. Kushnir, M. Visbeck, N. Naik, J. Miller, G. Krahmann, H. Cullen, 2000: Causes of Atlantic Ocean climate variability between 1958 and 1998. *J. Climate*, **13**, 2845–2862.

Speer, K., E. Tziperman, 1992: Rates of Water Mass Formation in the North Atlantic Ocean, Speer, K., *J. Phys. Ocean.*, **25**(01), 93–104.

Stommel, H., 1995: Determination of water mass properties of water pumped down from the Ekman layer to the geostrophic flow below, Stommel, H., *Collected Works of Henry Stommel*, II-207,II-211,Vol. II,Chap. 1.

Walin, G., 1982: On the relation between sea-surface heat flow and thermal circulation in the ocean. *Tellus*, **34**, 187–195.

Williams, R. G., Ocean subduction, 2001: *Science*, **109**, 10,1982–1983.

Worthington, L., 1959: The 18^o water in the Sargasso Sea. *Deep-Sea Res.*, **5**, 297–305.

Wu, L. and Z. Liu, 2005: North Atlantic Decadal Variability: AirSea Coupling, Oceanic Memory, and Potential Northern Hemisphere Resonance. *J. Climate*, **18**, 331–349.

Wunsch, C., 1999: Where do ocean eddy heat fluxes matter?, *J. Geophys. Res.*, **104**(13), 235–249.

Xie, S.-P., 2004: Satellite observations of cool ocean-atmosphere interaction, Xie, S.-P., *Bull. Amer. Meteor. Soc.*, **85**(02),195–208.

School of Oceanography, Box 355351, University of Washington, Seattle, WA 98195.

trossd@u.washington.edu

Received _____

Figure Captions

Figure 1. Mean annual geostrophic and ageostrophic (as estimated from the first-order quasi-geostrophic equations described in the Appendix) currents from Aviso in the Gulf Stream region from 1999 to 2006.

Figure 2. The atmosphere, surface Ekman layer, mixed layer, seasonal thermocline, and permanent thermocline are shown. The gray parallelograms are approximate representations of the water columns that either subduct or obduct. Here, h_m is the boundary between the seasonal and permanent thermocline. In the top case, the water column subducts and stays in the permanent thermocline. In the bottom case, the water column obducts. The dashed arrow indicates time evolution.

Figure 3. The MLDs in March (top), their associated errors (center), and the month numbers (e.g. March $= 3$) when the MLDs reach a maximum in late winter/early spring of 2004 (left) and 2006 (right). These are the years with the most spatial coverage by Argo floats and the one with the least, respectively, since WMO 852 float errors were introduced.

Figure 4. The mean annual Ekman pumping [in $\frac{m}{yr}$] in the Gulf Stream and Sargasso Sea regions, including currents (solved numerically) from 1999 to 2006 (top) and the difference between the mean annual w_e [in $\frac{m}{yr}$] in the same region including currents and that without currents (bottom).

Figure 5. The mean annual subduction [in $\frac{m}{yr}$] (left) and obduction [in $\frac{m}{yr}$] (right) rates for 2002-2003 (top), 2003-2004 (second to top), 2004-2005 (second to bottom), and 2005-2006 (bottom) using monthly-varying MLDs and weekly-varying currents with shear.

Figure 6. The mean annual subduction [in $\frac{m}{yr}$] (left) and obduction [in $\frac{m}{yr}$] (right) rates using a climatology with 2002-2007 average monthly-varying MLDs and 1999-2006 average currents: with shear (top) and without shear (bottom) in the currents.

Figure 7. The mean subduction [in $\frac{m}{yr}$] (left) and obduction [in $\frac{m}{yr}$] (right) rates over 2002-2006 using mean velocities and mean MLDs (top), using mean velocities and estimated monthly MLDs (middle), and using estimated weekly velocities and estimated monthly MLDs (bottom), all with shear.

Figure 8. Volume transports [in Sv] categorized into subduction (gray positive bars), EDW subduction (black positive bars), obduction (gray negative bars), and EDW obduction (black negative bars), broken into intervals of $0.2\frac{kg}{m^3}$ for 2002 (top left), 2003 (top right), 2004 (bottom left), and 2005 (bottom right).

Figure 9. Locations of where at least 90% of the heavy, $27.0\frac{kg}{m^3}$ and above, water [x] and light, $22.0\frac{kg}{m^3}$ and below, water [o] subducts for (a) 2002, (b) 2003, (c) 2004, and (d) 2005.

Figure 10. Thickness of waters between 17 and 19^oC [in meters] in springtime (April-June) with locations where at least 90% of EDW subduction occurs [diamond] in (a) 2002, (b) 2003, (c) 2004, and (d) 2005.

Tables

Table 1. The data we used in our calculations

Quantity	Winds	SSH	MLD, σ_θ, EDW, shear	shear	NAO indices
Source	QuikSCAT	Aviso	Argo, WOCE/ACCE	WOA	
Dates	Jan 02-Aug 06	Jan 02-Aug 06	Jan 02-Jun 07	pre-1994	
Frequency	daily	weekly	every 10 days	monthly	

Table 2. Root mean squared (rms) and maximum subduction, obduction, and error: 'analytical' ($\frac{1}{T}\Delta h$ from *Qiu and Huang* (1995)) versus modeled ['-' is insufficient data]

estimation	2002	2003	2004	2005	2006
Analytical error maximum [$\frac{m}{year}$]	110	150	180	140	120
Analytical error rms [$\frac{m}{year}$]	70	90	100	80	65
Analytical subduction maximum [$\frac{m}{year}$]	450	460	1100	780	650
Analytical subduction rms [$\frac{m}{year}$]	90	100	230	150	75
Modeled subduction maximum [$\frac{m}{year}$]	220	460	640	620	-
Modeled subduction rms [$\frac{m}{year}$]	60	70	130	120	-
Modeled obduction maximum [$\frac{m}{year}$]	420	330	680	680	-
Modeled obduction rms [$\frac{m}{year}$]	120	90	130	150	-

Table 3. Ventilation and EDW rates and EDW volume from 2002 to 2006 ['-' is insufficient data]

mean annual	2002	2003	2004	2005	2006
Volume $17-19^{o}$C water [10^{14} m^3]	15.8	20.2	17.8	22.0	21.3
EDW volume (below h_m) [10^{14} m^3]	9.6	6.0	5.1	7.4	6.6
EDW subduction rate [Sv]	2.3	1.0	0.33	0.72	-
EDW obduction rate [Sv]	1.8	1.3	2.3	3.8	-
Subduction [Sv]	37.3	52.2	65.4	52.6	-
Obduction [Sv]	65.8	73.9	60.5	63.3	-

Figures

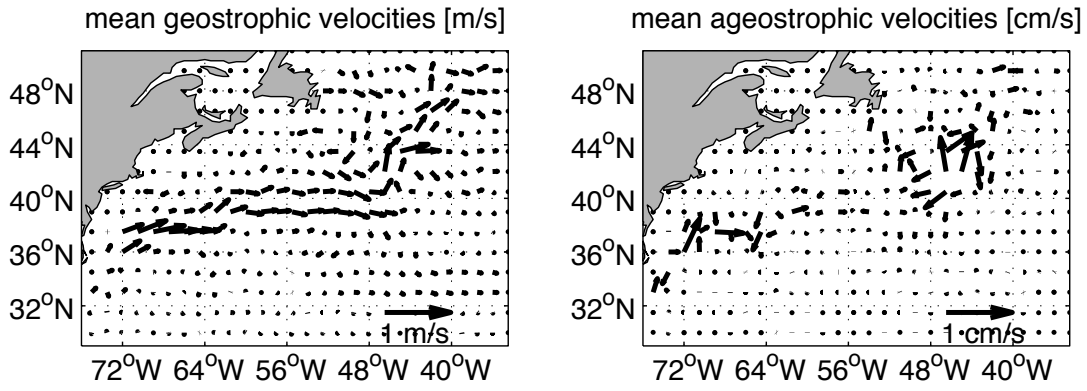

.

Figure 1. Mean annual geostrophic and ageostrophic (as estimated from the first-order quasi-geostrophic equations described in the Appendix) currents from Aviso in the Gulf Stream region from 1999 to 2006.

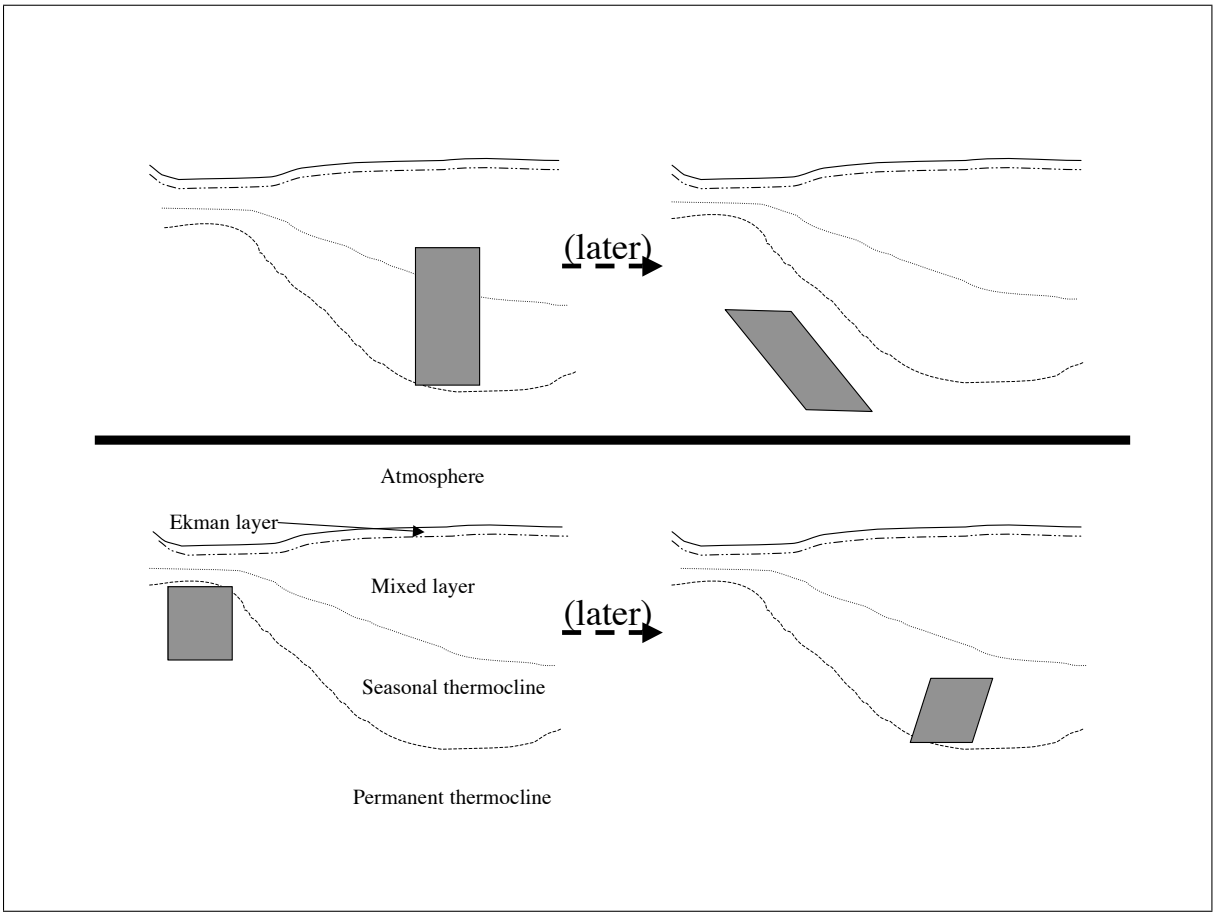

Figure 2. The atmosphere, surface Ekman layer, mixed layer, seasonal thermocline, and permanent thermocline are shown. The gray parallelograms are approximate representations of the water columns that either subduct or obduct. Here, h_m is the boundary between the seasonal and permanent thermocline. In the top case, the water column subducts and stays in the permanent thermocline. In the bottom case, the water column obducts. The dashed arrow indicates time evolution.

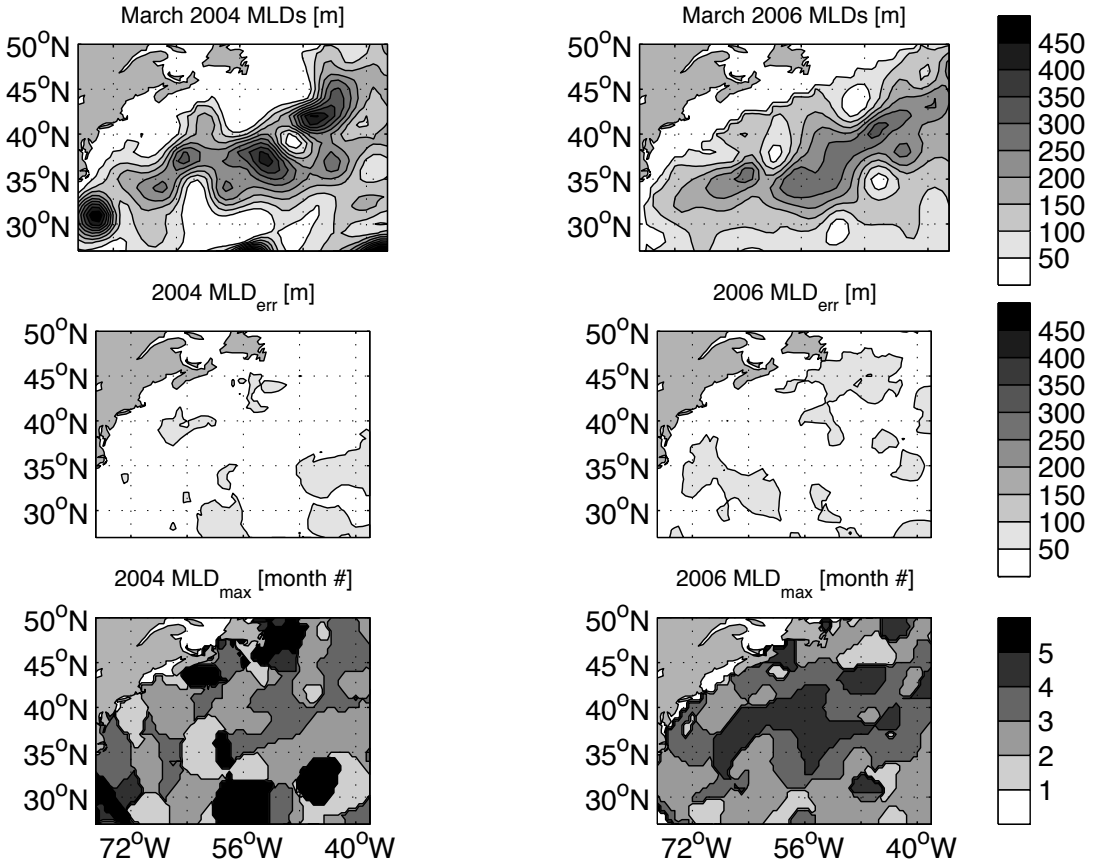

Figure 3. The MLDs in March (top), their associated errors (center), and the month numbers (e.g. March $= 3$) when the MLDs reach a maximum in late winter/early spring of 2004 (left) and 2006 (right). These are the years with the most spatial coverage by Argo floats and the one with the least, respectively, since WMO 852 float errors were introduced.

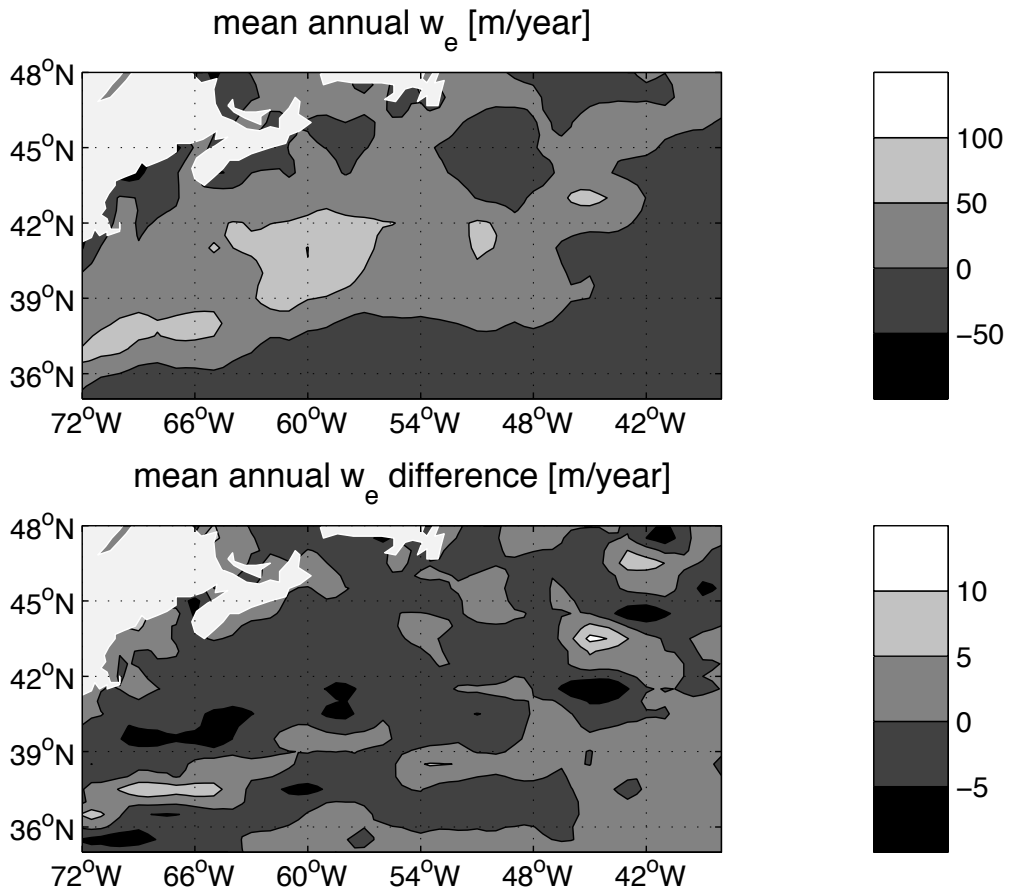

Figure 4. The mean annual Ekman pumping [in $\frac{m}{yr}$] in the Gulf Stream and Sargasso Sea regions, including currents (solved numerically) from 1999 to 2006 (top) and the difference between the mean annual w_e [in $\frac{m}{yr}$] in the same region including currents and that without currents (bottom).

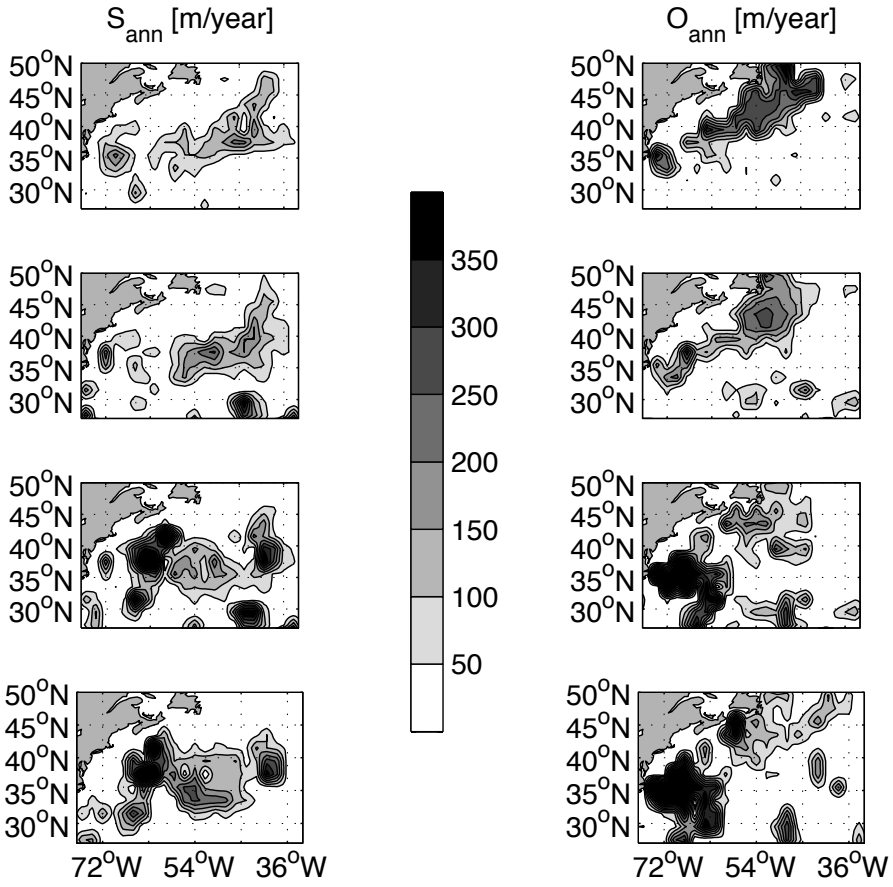

Figure 5. The mean annual subduction [in $\frac{m}{yr}$] (left) and obduction [in $\frac{m}{yr}$] (right) rates for 2002-2003 (top), 2003-2004 (second to top), 2004-2005 (second to bottom), and 2005-2006 (bottom) using monthly-varying MLDs and weekly-varying currents with shear.

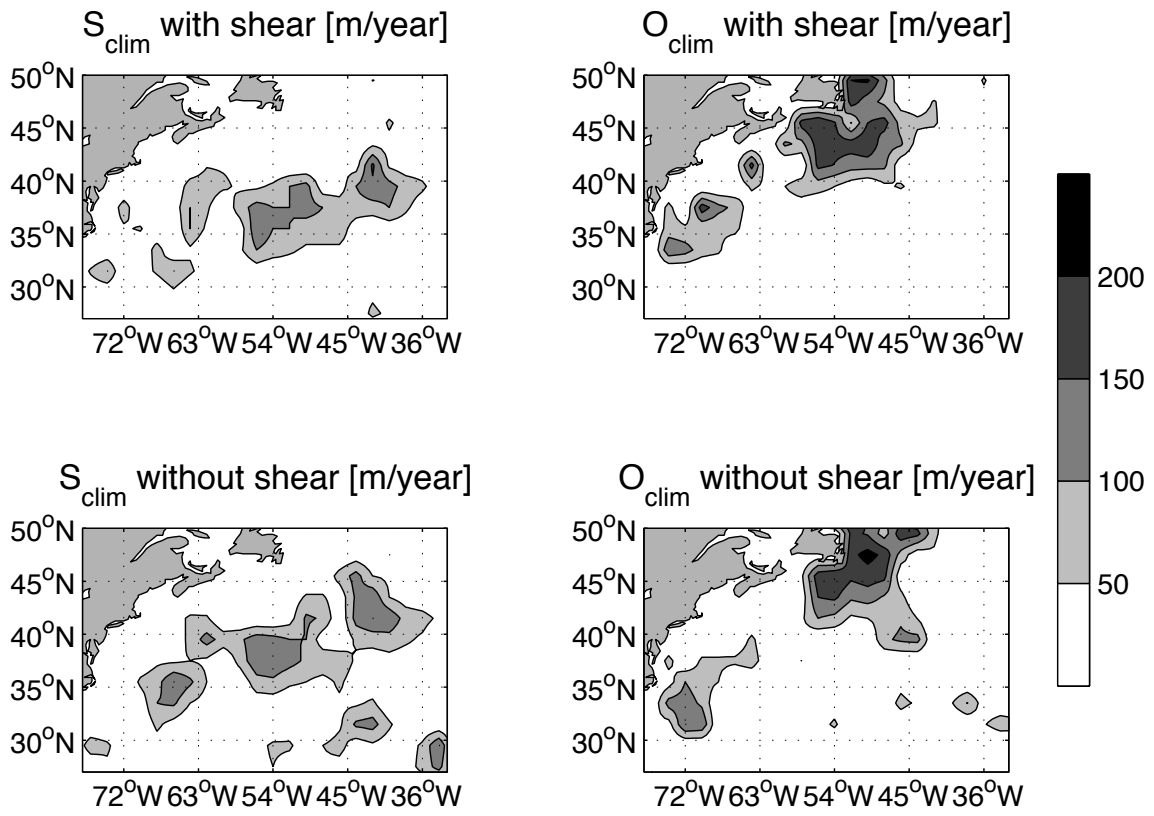

Figure 6. The mean annual subduction [in $\frac{m}{yr}$] (left) and obduction [in $\frac{m}{yr}$] (right) rates using a climatology with 2002-2007 average monthly-varying MLDs and 1999-2006 average currents: with shear (top) and without shear (bottom) in the currents.

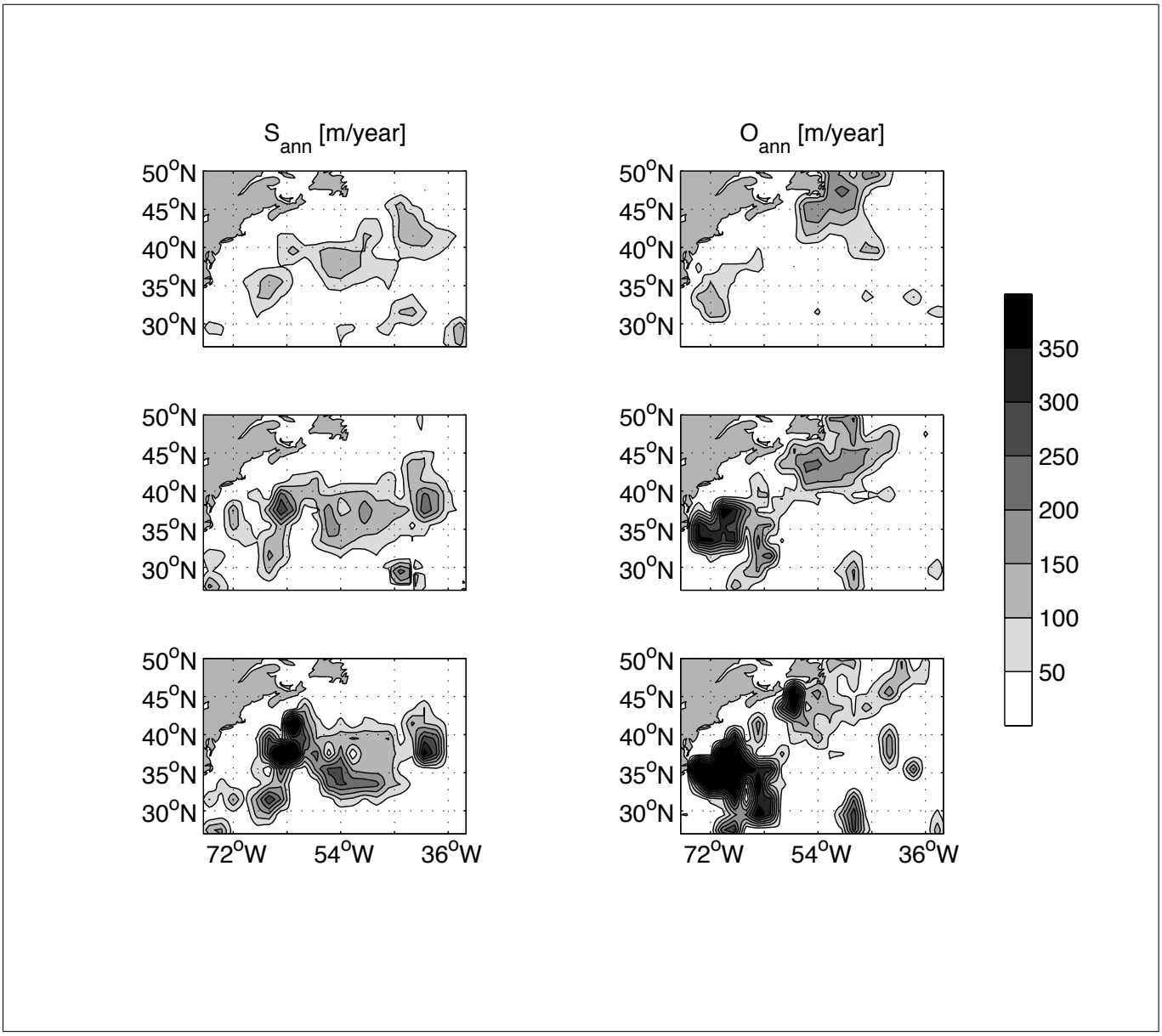

Figure 7. The mean subduction [in $\frac{m}{yr}$] (left) and obduction [in $\frac{m}{yr}$] (right) rates over 2002-2006 using mean velocities and mean MLDs (top), using mean velocities and estimated monthly MLDs (middle), and using estimated weekly velocities and estimated monthly MLDs (bottom), all with shear.

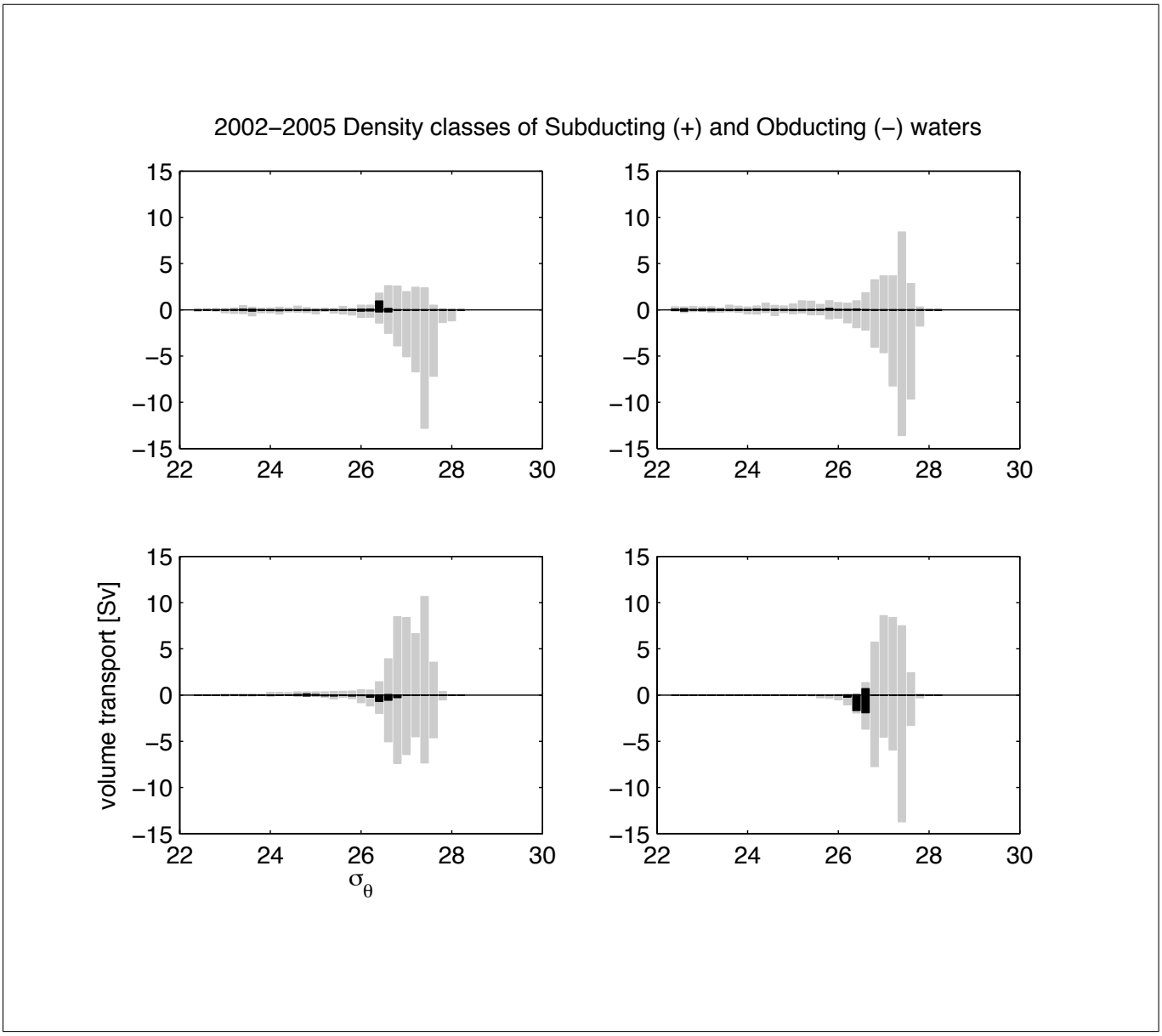

Figure 8. Volume transports [in Sv] categorized into subduction (gray positive bars), EDW subduction (black positive bars), obduction (gray negative bars), and EDW obduction (black negative bars), broken into intervals of $0.2\frac{kg}{m^3}$ for 2002 (top left), 2003 (top right), 2004 (bottom left), and 2005 (bottom right).

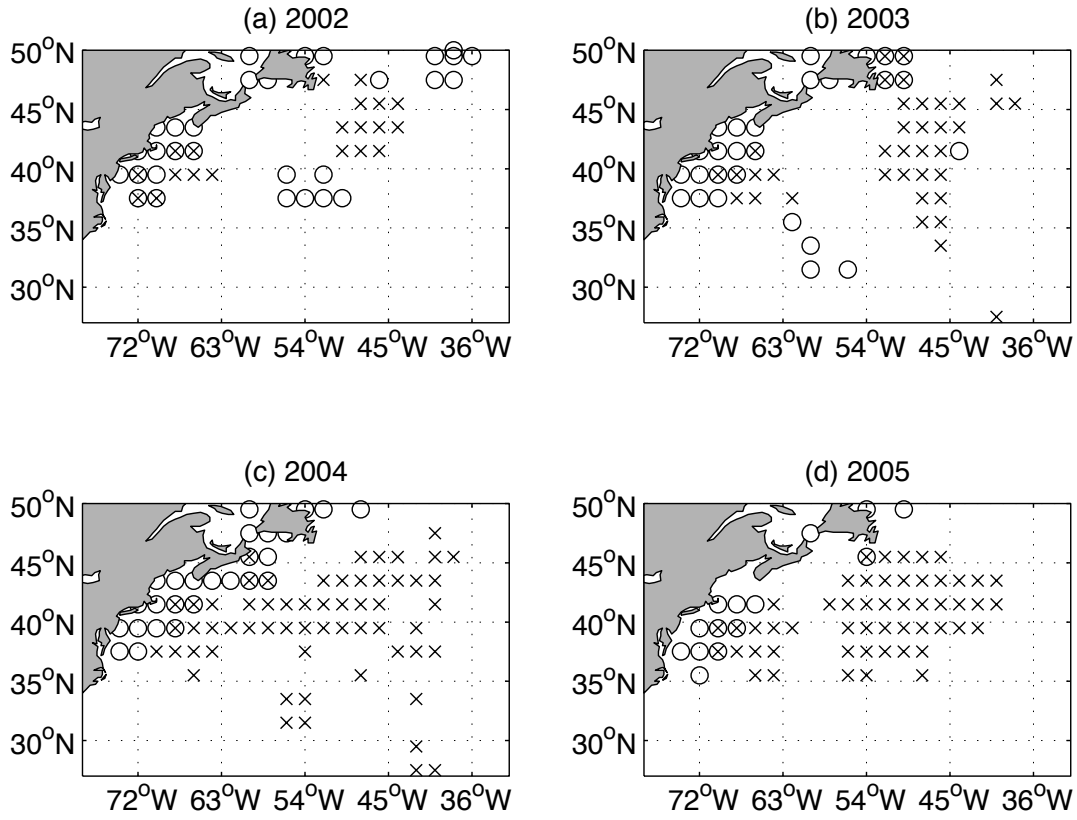

Figure 9. Locations of where at least 90% of the heavy, $27.0\frac{kg}{m^3}$ and above, water [x] and light, $22.0\frac{kg}{m^3}$ and below, water [o] subducts for (a) 2002, (b) 2003, (c) 2004, and (d) 2005.

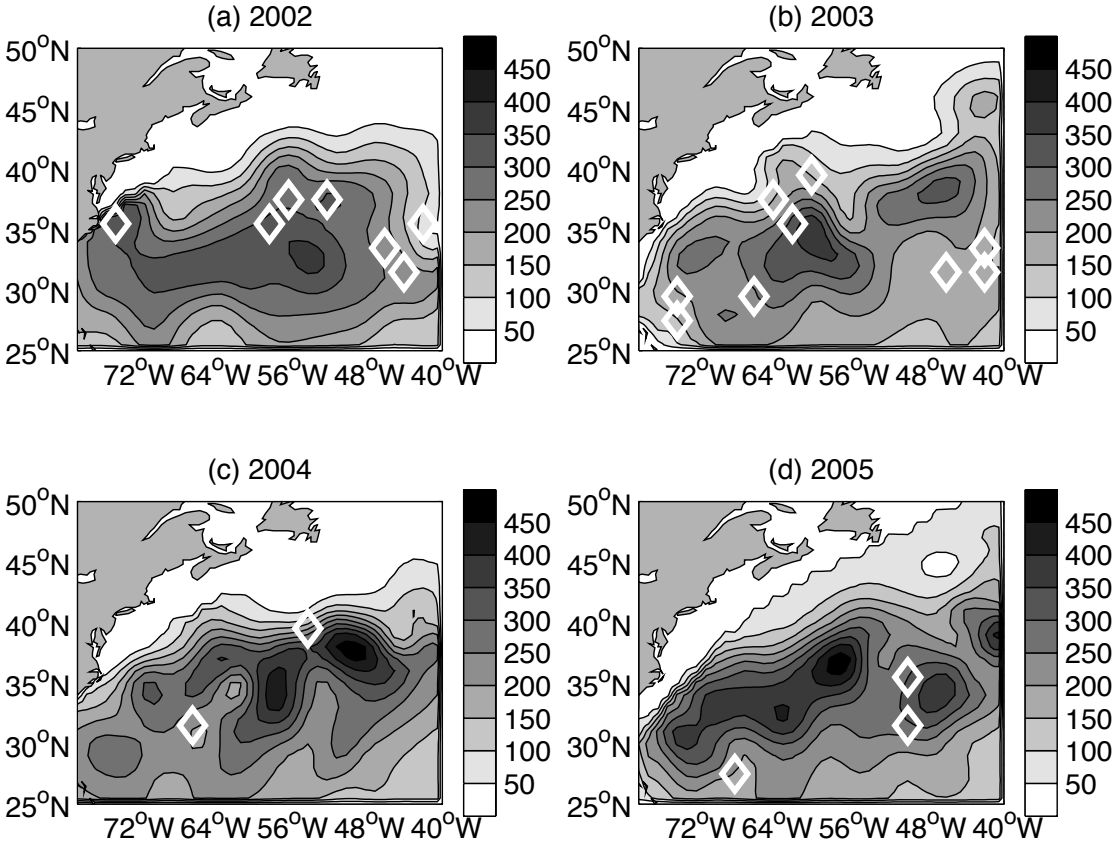

Figure 10. Thickness of waters between 17 and 19°C [in meters] in springtime (April-June) with locations where at least 90% of EDW subduction occurs [diamond] in (a) 2002, (b) 2003, (c) 2004, and (d) 2005.